Supporting Information

Vinylene-Linked Covalent Organic Frameworks with Fully Pyridine-Patterned Iso-π-Conjugation for Photoredox Catalysis

Fancheng Meng,[a] Zixing Zhang, [a] Xiaomeng Li, [a] Lingjun Zeng, [a] Bai Xue, *, [a] Biao Jiang, [a] Xin Jin,*, [a] Jindong Wu, [a] Jianneng Li, [b] Kui Yang,[b] and Fan Zhang*, [a]

[a] School of Chemistry and Chemical Engineering, State Key Laboratory of Synergistic Chem-Bio Synthesis, Shanghai Jiao Tong University, Shanghai 200240, China. E-mail: bxue79@sjtu.edu.cn; jxcindy@sjtu.edu.cn; fan-zhang@sjtu.edu.cn

[b] Yunnan Advanced Elastomer Industry Innovation Research Institute Co., Ltd. P. R. China

Experimental section

Materials. 2,4,6-Trimethylpyridine, 2,2'-bipyridyl-5,5'-dialdehyde, and were purchased from Adamas Reagent, Ltd. Benzoic anhydride and benzoic acid were obtained from the Acros Organics. 2,2',6,6'-tetramethyl-4,4'-bipyridine were synthesized according to literature method. All the common solvents including petroleum ether, dichloromethane, ethyl acetate, tetrahydrofuran, and methanol were also purchased from Adamas Reagent, Ltd. Anhydrous *N*, *N*-Dimethylformamide (DMF) were purchased form J&K Scientific (Beijing, China). All the chemicals were commercially available directly used without further purification.

Characterization. The reactions involving inert atmosphere were carried out using standard Schlenk technique or in an MBraun glovebox. Solution nuclear magnetic resonance measurements were performed on a Bruker 400 (400 MHz for proton, 100 MHz for carbon) spectrometer with tetramethyl silane as the internal reference using chloroform-d_3 or dichloromethane-d_2 as solvent. The Fourier transform infrared (FT-IR) spectra were obtained on a Nicolet 670 FT-IR spectrometer. X-ray diffraction (XRD) measurements were performed on a Bruker D8 Advance diffractometer with CuKα1 radiation (λ = 1.54006 Å). N_2 adsorption-desorption isotherms were measured on an ASAP 2020 PLUS HD88 apparatus at 77K and the surface areas were calculated by the Brunauere Emmette Teller (BET) method. The pore size distribution was calculated by nonlocal density functional theory (NLDFT). Ultraviolet-visible reflectance spectrum (UV-vis DRS) absorption spectra were collected using a Shimadzu UV-2600 UV-vis spectrophotometer. Electron paramagnetic response (EPR) spectra were obtained using a Bruker ELEXSYS Ⅱ E 500 EPR Spectrometer at room temperature. The scanning emission microscope (SEM) measurements were conducted using a FEI Nova NanoSEM 230 Field Emission Scanning Electron Microscope. High-resolution transmission electron microscopy (TEM) images were obtained using a FEI Super-X field emission transmission electron microscope operating at an accelerating voltage of 5.0 kV.

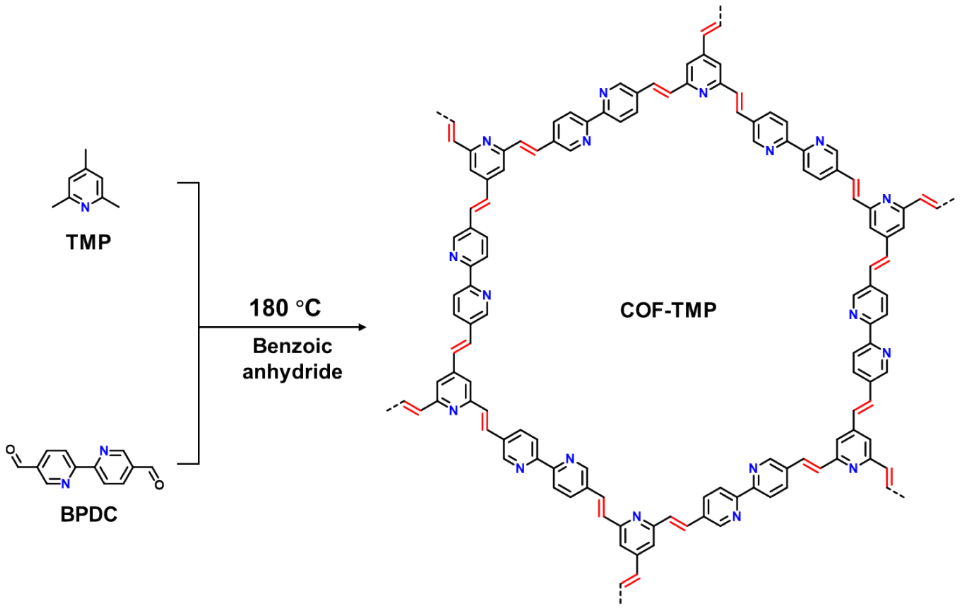

Synthesis of COF-TMP. 2,4,6-Trimethylpyridine (48.47 mg, 0.4 mmol) and 2,2'-bipyridine-5,5'-dicaraldehyde (169.77 mg, 0.6 mmol) were added in a 10 mL Pyrex tube containing benzoic anhydride (180.98 mg, 0.8 mmol). The tube was frozen at 77K using liquid N_2 and degassed by three freeze-pump-thaw cycles, sealed under vacuum, and then sealed and heated in an oven at 180 °C for 3 days. After cooling down to room temperature, a yellow solid was collected and washed with tetrahydrofuran and methanol. The resulting COF was obtained as yellow powder in a yield of 88.7%.

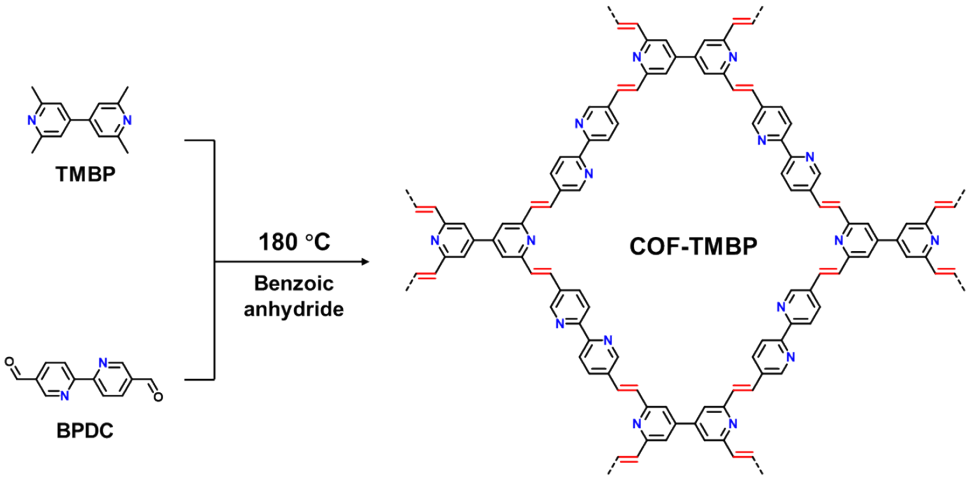

Synthesis of COF-TMBP. By means of the synthesis produce for COF-TMP with TMBP (84.92 mg, 0.4 mmol) instead of TMP (48.47 mg, 0.4 mmol), COF-TMBP was obtained as yellow powder in a yield of 92.3%.

Photoelectrochemical measurements.

Photocurrents, electrochemical impedance spectroscopy (EIS) and Mott-Schottky (MS) curves measurement. Working photoelectrode is constructed by the as-prepared COFs

powder and Nafion solution (5 wt%). Specifically, COF powder (5 mg) and Nafion (100 μL) were blended into DMF (900 μL) as stock solution. Subsequently, the as-prepared slurry (100 μL) was drop-coated on a clean ITO glass, and the COF-based photoelectrode can be obtained by drying the DMF in ambient condition. These measurements were conducted on a CHI 760E electrochemical work station in a three-electrode cell system under irradiation of a 300 W Xe lamp (Perfect Light PLS-SXE200/300UV) with a 420 nm cutoff filter. Transient photocurrent response, linear sweep voltammetry (LSV), and Mott-Schottky of electrochemical impedance spectroscopy (EIS) were conducted by a three-electrode system, using COF-based electrode as working electrode, Pt foil (1.0×1.0 cm^2) as counter electrode, and Ag/AgCl as reference. Especially, the flat band potential can be obtained by plotting the tangent line of Mott-Schottky spectra. The intersection point of the tangent line and a-axis can be applied as the conduction band. The applied potentials vs. Ag/AgCl are converted to RHE potentials using the following equation:

$E_{RHE} = E_{Ag/AgCl} + 0.0591pH + E^{\theta}_{Ag/AgCl}$ ($E^{\theta}_{Ag/AgCl} = 0.199$ V)

Typical procedure for photocatalytic synthesis of 2-substituted benzothiazoles

2-Aminobenzenethiol or its derivatives (0.4 mmol), acetaldehyde or aromatic aldehyde (0.4 mmol), COFs (10 mg, 5 mol%), and anhydrous ethanol (10.0 mL) were added into a reaction tube. The reaction mixture was opened to air and stirred at room temperature under 10 W blue LEDs (the distance between LEDs and reaction tube is about 10 cm). The progress of the reaction was monitored by TLC. After the reaction was completed, the heterogeneous catalyst could be isolated through filtration and thoroughly washed by acetone (4 mL $\times$ 3). The combined organic phase was evaporated at reduced pressure, and the residue was further purified by flash column chromatography with petroleum/dichloromethane = 1/1 as eluent to give the target 2-substituted benzothiazoles.

Supplementary figures and tables

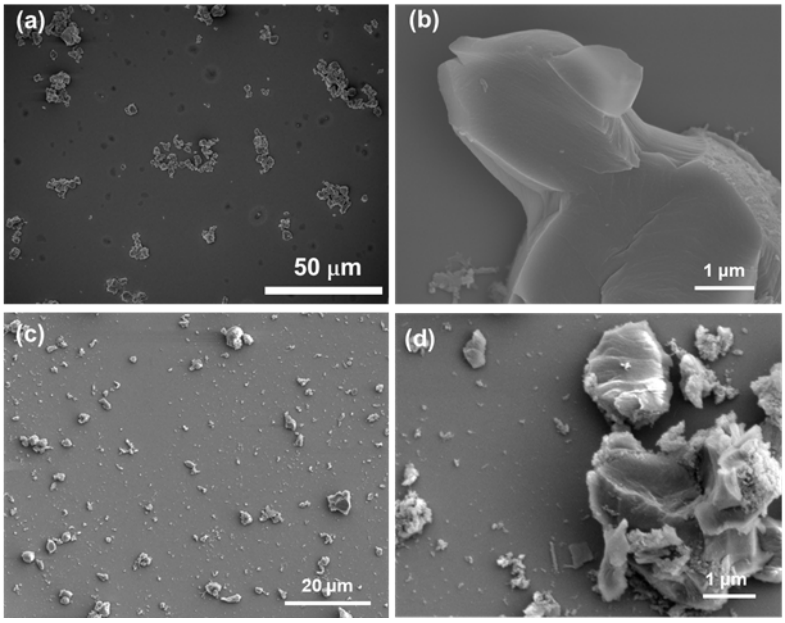

Figure S1. SEM images of (a, b) COF-TMP and (c, d) COF-TMBP.

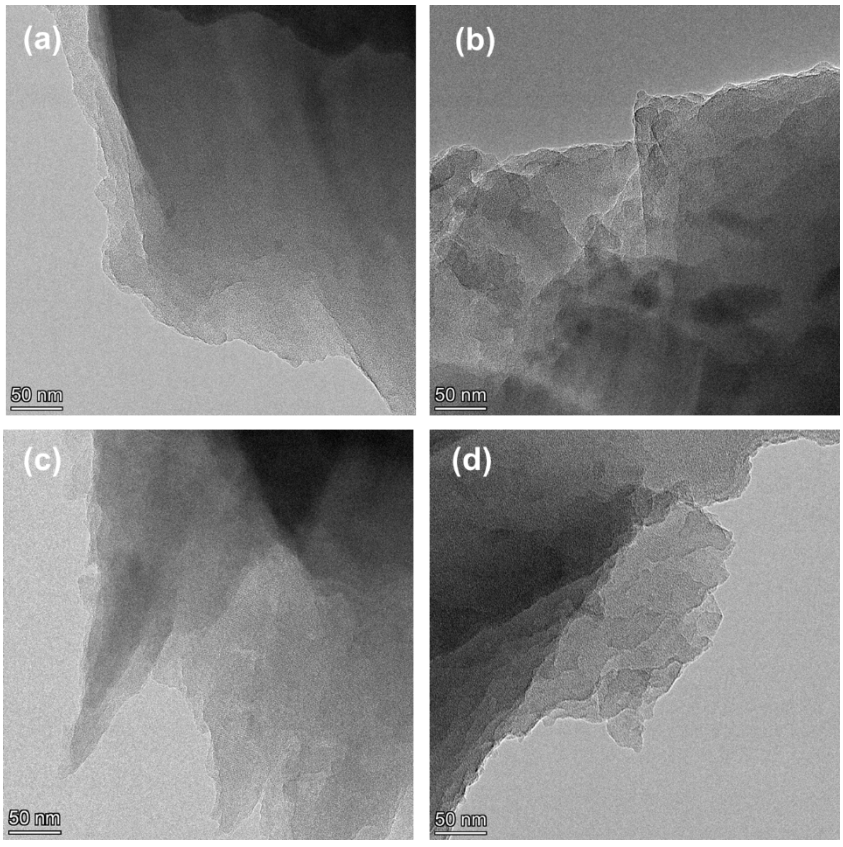

Figure S2. TEM images of (a, b) COF-TMP and (c, d) COF-TMBP.

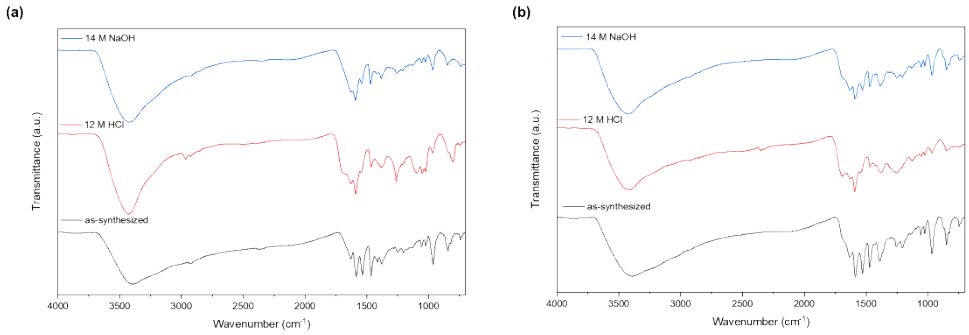

Figure S3. FT-IR spectra of (a) COF-TMP and (b) COF-TMBP after treating the COFs with harsh conditions.

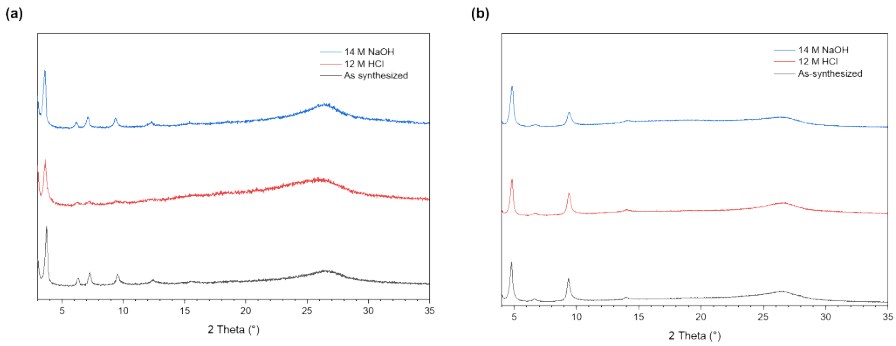

Figure S4. PXRD patterns of (a) COF-TMP and (b) COF-TMBP soaked in aqueous solution of NaOH (14_M) or HCl (12_M) for two weeks.

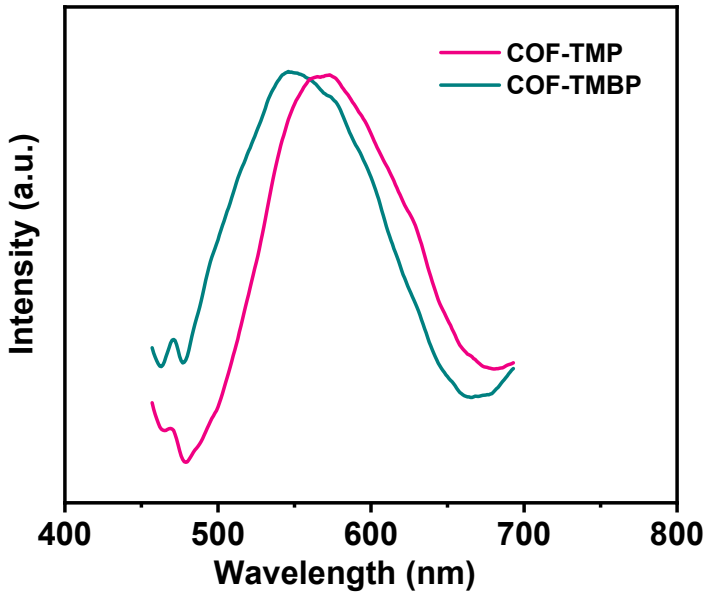

Figure S5. Steady-state photoluminescence (PL) of COF-TMP and COF-TMBP.

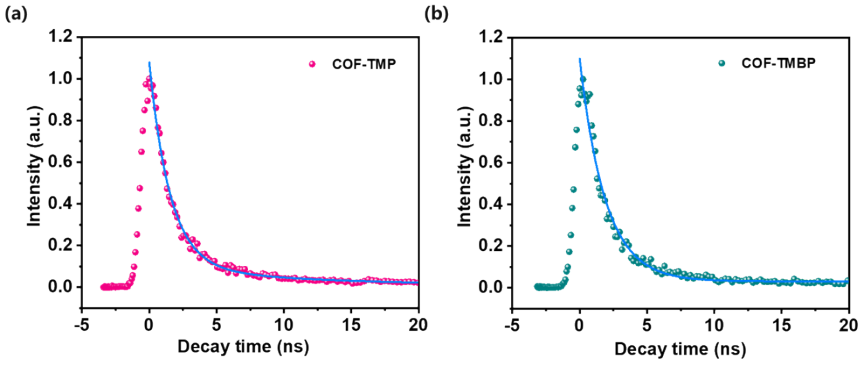

Figure S6. Time-resolved photoluminescence (PL) spectrum of the (a) COF-TMP and (b) COF-TMBP.

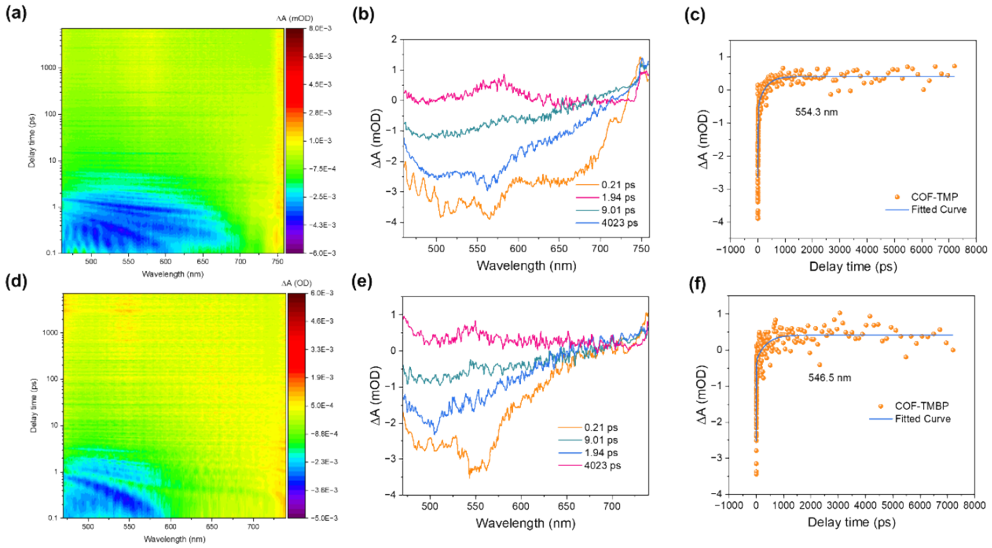

Figure S7. Photogenerated carrier dynamics. fs-TA spectra excited at 400 nm of (a) COF-TMP and (d) COF-TMBP. Corresponding spectra of (b) COF-TMP and (e) COF-TMBP at selected pump−probe time delays. Decay kinetic curves of (c) COF-TMP probed at 554 nm and (f) COF-TMBP probed at 547 nm.

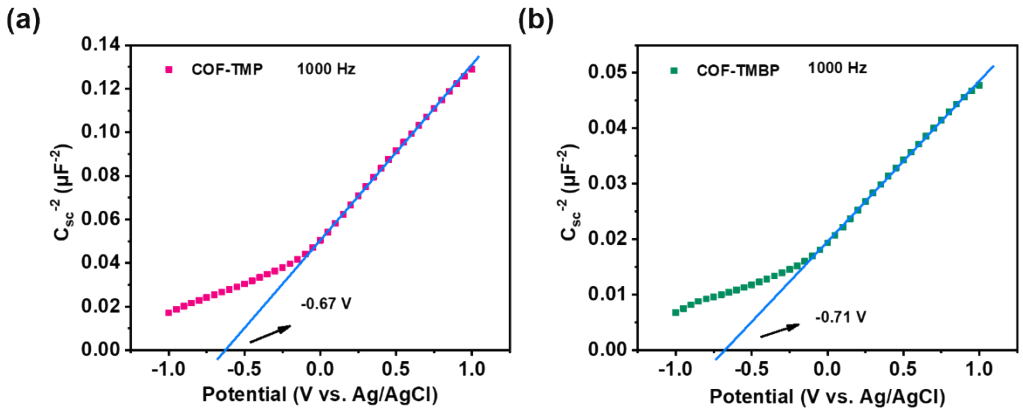

Figure S8. Mott-Schottky plots of the (a) COF-TMP and (b) COF-TMBP in 0.2 M Na_2SO_4

aqueous solution (pH = 6.8).

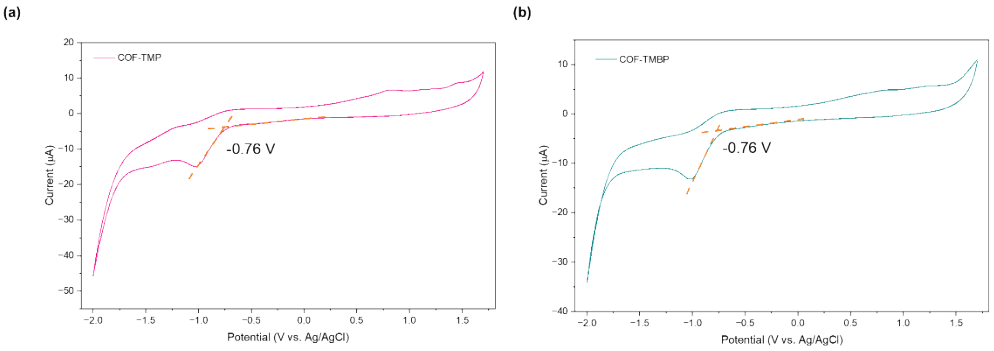

Figure S9. (b) Cyclic voltammograms of COF-TMP and COF-TMBP measured at 298 K in dichloromethane using tetrabutylammonium hexafluorophosphate ($TBAPF_6$) as the electrolyte (100 mM) with a scan rate of 0.1 $V \cdot s^{-1}$ from -2.0 to 1.7 V. Potentials were evaluated by (E_{ox} + E_{red})/2. Fc = ferrocene.

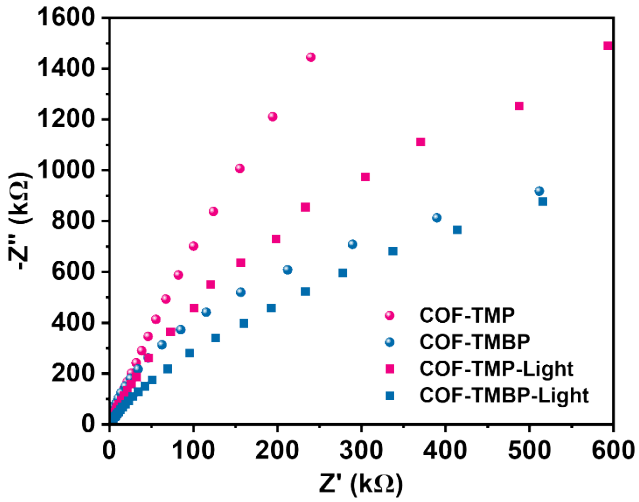

Figure S10. Electrochemical impedance spectroscopy (EIS) Nyquist plots of COF-TMP and COF-TMBP film photoelectrodes with and without light irradiation.

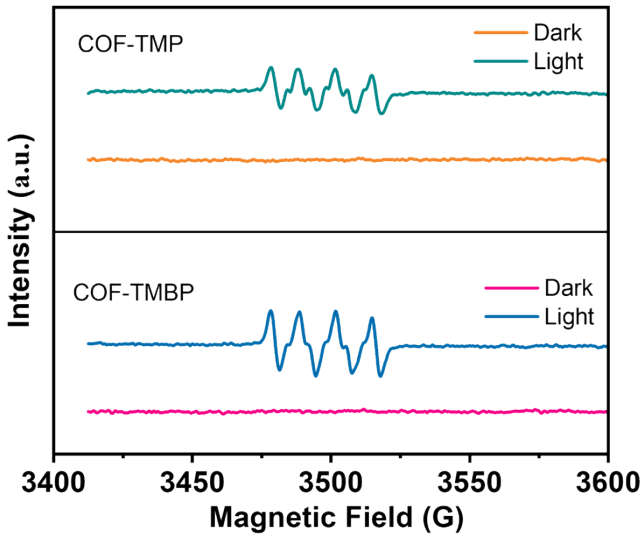

Figure S11. EPR spectra of COF-TMP and COF-TMBP in the dark and under illumination for 2 min using 5,5-dimethyl-1-pyrroline (DMPO) as a spin-trap agent.

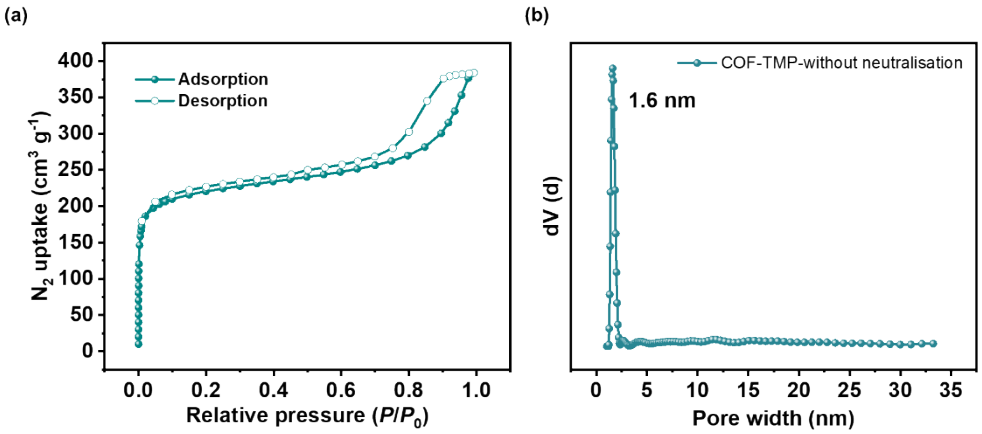

Figure S12. (a) Nitrogen adsorption-desorption isotherm and (b) pore size distribution of the COF-TMP without neutralization treatment.

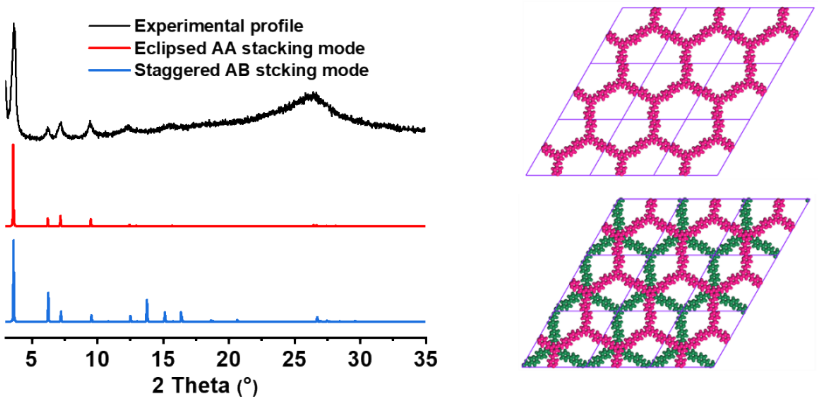

Figure S13. Powder X-ray diffraction (PXRD) patterns for COF-TMP: experimental profile

(black), and the simulated curves for the eclipsed AA stacking mode (red) and AB stacking mode (blue).

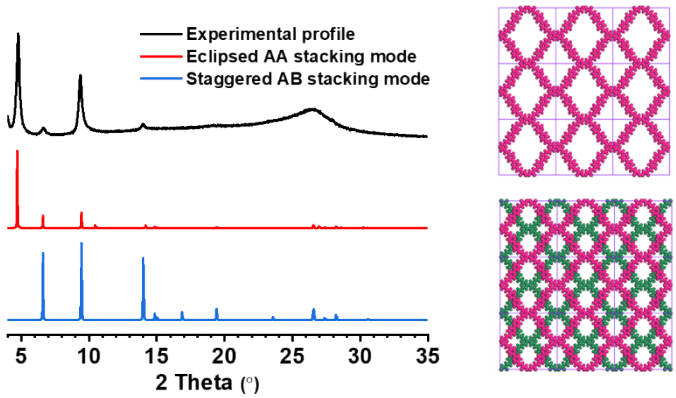

Figure S14. Powder X-ray diffraction (PXRD) patterns for COF-TMBP: experimental profile (black), and the simulated curves for the eclipsed AA stacking mode (red) and AB stacking mode (blue).

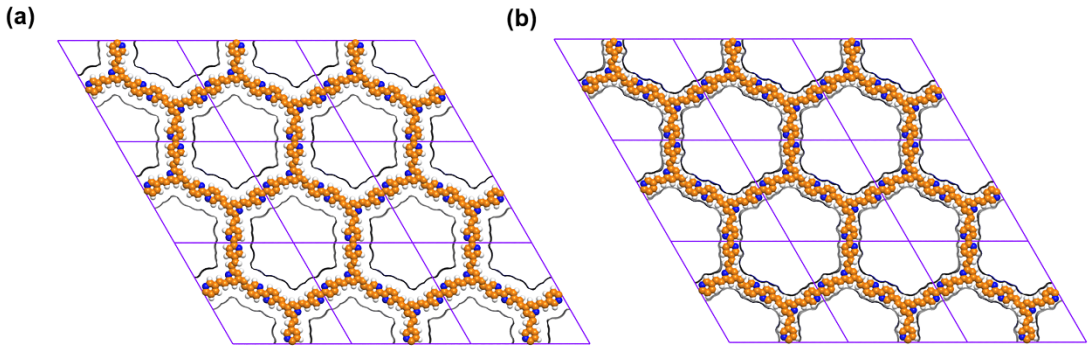

Figure S15. (a) Solvent accessible surface and (b) Connolly surface of COF-TMP. (probe radius for N_2 of 1.84 Å). Carbon, hydrogen and nitrogen atoms are presented as orange, white and blue spheres, respectively.

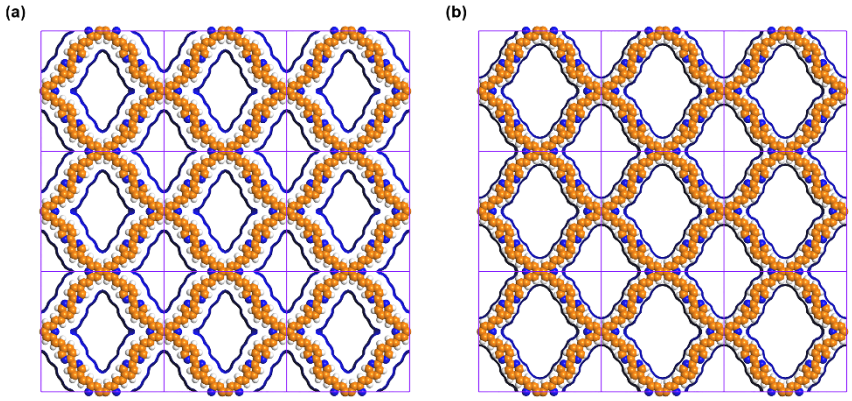

Figure S16. (a) Solvent accessible surface and (b) Connolly surface of COF-TMBP. (probe radius for N_2 of 1.84 Å). Carbon, hydrogen and nitrogen atoms are presented as orange, white and blue spheres, respectively.

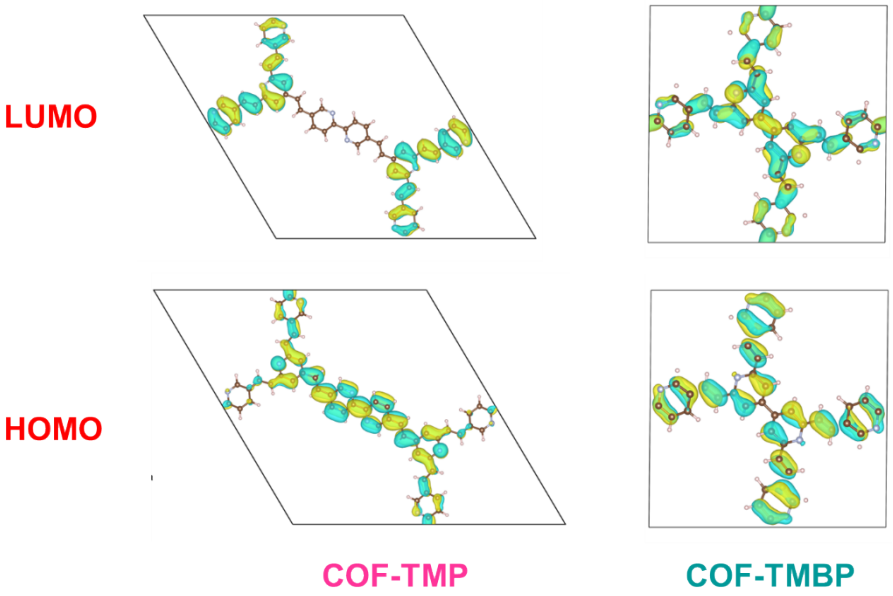

Figure S17. The HOMO and LUMO of the COF-TMP and COF-TMBP.

Table S1. Comparison of the full width at half-maximum (FWHM) of the strongest diffraction peak of the vinylene-linked COFs.

COFs	$FWHM_{100}$	reference
g-C40N3-COF	0.305°	*Nat. Commun.* **2019**, *10*, 2467.
g-C31N3-COF	0.884°	*Nat. Commun.* **2019**, *10*, 2467.
g-C37N3-COF	0.934°	*Nat. Commun.* **2019**, *10*, 2467.
g-C34N6-COF	0.882°	*Angew. Chem. Int. Ed.* **2019**, *58*, 12065-12069.
g-C18N3-COF	0.335°	*J. Am. Chem. Soc.* **2019**, *141*, 14272-14279.
g-C33N3-COF	0.707°	*J. Am. Chem. Soc.* **2019**, *141*, 14272-14279.
COF-1	0.3°	*Angew. Chem. Int. Ed.* **2019**, *58*, 13753-13757.
COF-2	0.45°	*Angew. Chem. Int. Ed.* **2019**, *58*, 13753-13757.
g-C30N6-COF	0.661°	*Sci. Bull.* **2020**, *65*, 1659-1666.
g-C48N6-COF	0.606°	*Sci. Bull.* **2020**, *65*, 1659-1666.
COF-p-3Ph	0.317°	*J. Am. Chem. Soc.* **2020**, *142*, 11893-11900.
COF-p-2Ph	0.463°	*J. Am. Chem. Soc.* **2020**, *142*, 11893-11900.
COF-m-3Ph	0.563°	*J. Am. Chem. Soc.* **2020**, *142*, 11893-11900.

g-C54N6-COF	0.513°	*Angew. Chem. Int. Ed.* **2020**, *59*, 23845-23853.
g-C52N6-COF	0.348°	*Angew. Chem. Int. Ed.* **2020**, *59*, 23845-23853.
2D-PPQV1	1.37°	*Angew. Chem. Int. Ed.* **2020**, *59*, 23620-23625
2D-PPQV2	1.28°	*Angew. Chem. Int. Ed.* **2020**, *59*, 23620-23625
ivCOF-1-Br	0.738°	Angew. Chem. Int. Ed. 2021, *60*, 13614-13620
ivCOF-2-Br	0.528°	Angew. Chem. Int. Ed. 2021, *60*, 13614-13620
ivCOF-2-I	0.635°	Angew. Chem. Int. Ed. 2021, *60*, 13614-13620
COF-TMP	0.249°	This work
COF-TMBP	0.250°	This work

Table S2. The quality of the Rietveld refinement is described by the R-factor for the COFs.

Sample	R_{wp}	R_p
COF-TMP	8.65	6.65
COF-TMBP	9.86	5.84

Table S3. Substrate scopes of visible-light-induced condensation cyclization.

Substrate	Light	Atmosphere	Solvent	Time	Yield
2-aminophenol	420 nm	Air	EtOH	4 h	70%
2-aminothiophenol	420 nm	Air	EtOH	4 h	96%
o-phenylenediamine	420 nm	Air	EtOH	4 h	92%

Table S4. Summary of the performance of photocatalytic generation of benzothiazole derivatives.

Catalyst	Light	Atmosphere	Solvent	Time	Yield	Reference
CMP-Th-Ph-F	460 nm	O_2	MeOH	4 h	99%	*ACS Appl. Mater. Interfaces* 2023, 15, 2825−2831
MOH-Tf1Tf2	30 W blue light	O_2	MeOH/H_2O = 1/1	3 h	90%	J. Mater. Chem. A, 2025, 13, 14103
OZBT-COF	30 W blue LED lamp	Air	MeOH	3 h	95%	Chemical Engineering Journal, 2024, 501, 157486
COF-TMP	420 nm	Air	EtOH	2 h	96%	This work

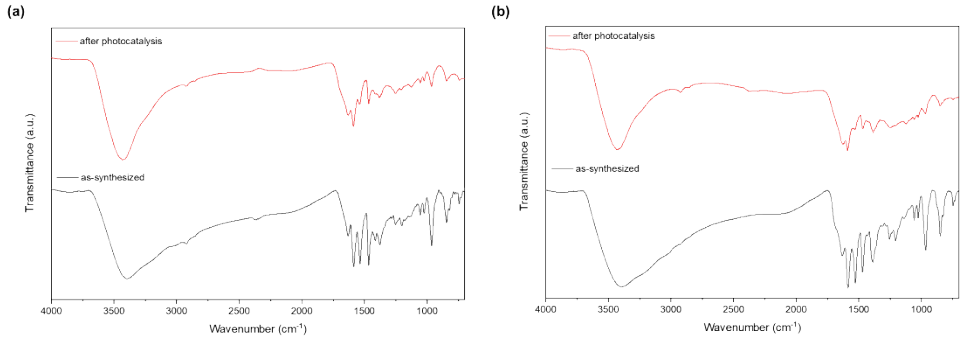

Figure S18. FTIR spectra of (a) COF-TMP and (b) COF-TMBP samples as-synthesized (black) and after photocatalytic tests (red).

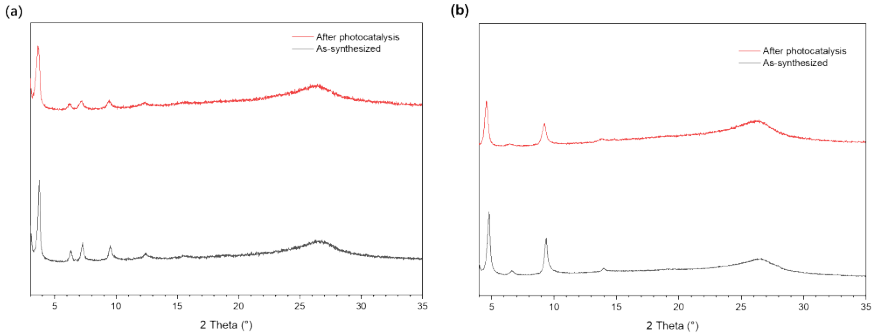

Figure S19. PXRD of (a) COF-TMP and (b) COF-TMBP samples as-synthesized (black) and after photocatalytic tests (red).

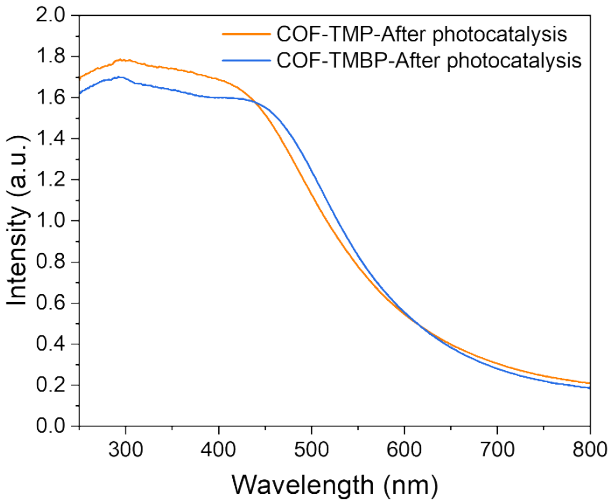

Figure S20. UV/vis diffuse reflectance spectra (DRS) of COF-TMP COF-TMBP after photocatalysis.

^{1}H NMR spectra and analysis of catalytic products

2-phenylbenzo[*d*]thiazole (3a): Prepared according to the typical procedure with 2-aminobenzenethiol and benzaldehyde derivatives. The crude product was purified by flash column chromatography on silica gel (petroleum ether/dichloromethane = 1/1 as eluent) to afford the product as a white solid (97% yield). ^{1}H NMR (400 MHz, $CDCl_3$) δ = 8.09 (m, 3H), 7.92 (d, 1H), 7.50 (m, 4H), 7.39 (t, 1H) ppm.

2-(p-tolyl)benzo[*d*]thiazole (3b): ^{1}H NMR (4000 MHz, $CDCl_3$) δ = 8.07 (d, 1H), 8.00 (d, 2H), 7.90 (d, 1H), 7.49 (t, 1H), 7.37 (t, 1H), 7.31 (d, 2H) ppm.

2-(4-methoxyphenyl)benzo[*d*]thiazole (3c): ^{1}H NMR (400 MHz, $CDCl_3$) δ = 8.05 (m, 3H), 7.88 (d, 1H), 7.47 (t, 1H), 7.35 (t, 1H), 7.01 (d, 2H) ppm.

2-(4-bromophenyl)benzo[*d*]thiazole (3d): ^{1}H NMR (400 MHz, $CDCl_3$): δ 8.09 (d, 1H), 7.98 (d, 2H), 7.92 (d, 1H), 7.64 (d, 2H), 7.51 (t, 2H) 7.41 (t, 1H) ppm.

4-(benzo[*d*]thiazol-2-yl)benzonitrile (3e): ^{1}H NMR (400 MHz, $CDCl_3$): 8.22 (d, 2H), 8.12 (d, 1H), 7.96 (d, 1H), 7.80 (d, 2H), 7.55 (t, 1H), 7.46 (t, 1H) ppm.

2-methylbenzo[*d*]thiazole (3f): ^{1}H NMR (400 MHz, $CDCl_3$) δ = 7.95 (d, 1H), 7.82 (d, 1H), 7.43 (t, 1H), 7.33 (t, 1H), 2.83 (s, 3H) ppm.

2,6-dimethylbenzo[1,2-*d*:4,5-*d*']bia(thiazole) (3i): ^{1}H NMR (400 MHz, $CDCl_3$): = 8.34 (s, 2H), 2.83 (s, 6H) ppm.

2-phenyl-1H-benzo[d]imidazole (3n): ^{1}H NMR (400 MHz, $CDCl_3$) d = 12.84 (s, 1H), 8.20 (m, 2H), 7.62 (d, 2H), 7.58 (m, 1H), 7.51 (t, 1H), 7.22 (m, 2H) ppm.

2-phenylbenzo[d]oxazole (3o): ^{1}H NMR (400 MHz, $CDCl_3$) d = 8.27 (d, 2H), 7.79 (d, 1H), 7.53 (d, 1H), 7.52 (m, 3H), 7.39 (t, 2H) ppm.

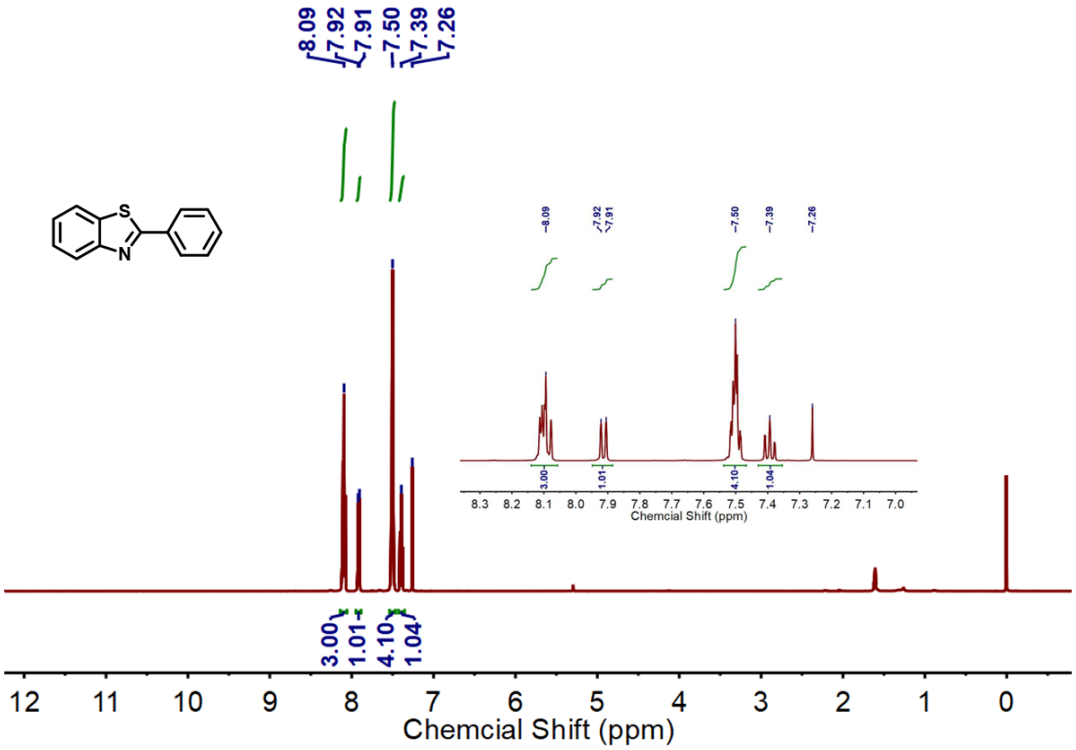

Figure S21. ^{1}H NMR spectrum of 2-phenylbenzo[*d*]thiazole (3a).

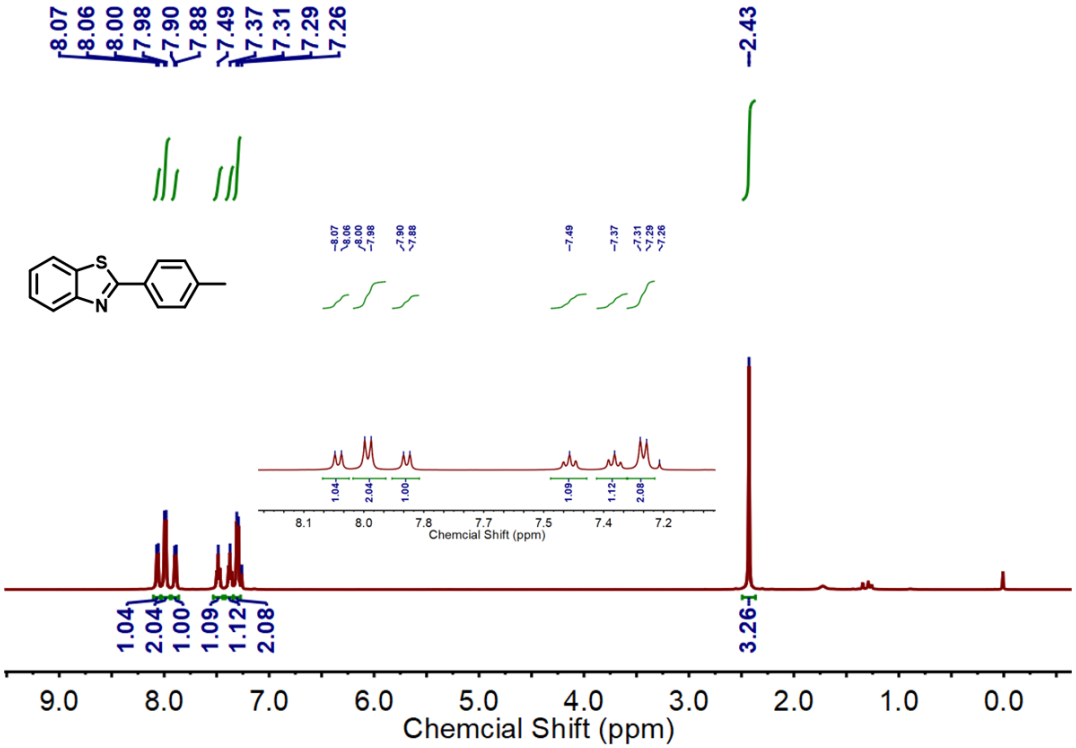

Figure S22. ^{1}H NMR spectrum of 2-(p-tolyl) benzo[*d*]thiazole (3b).

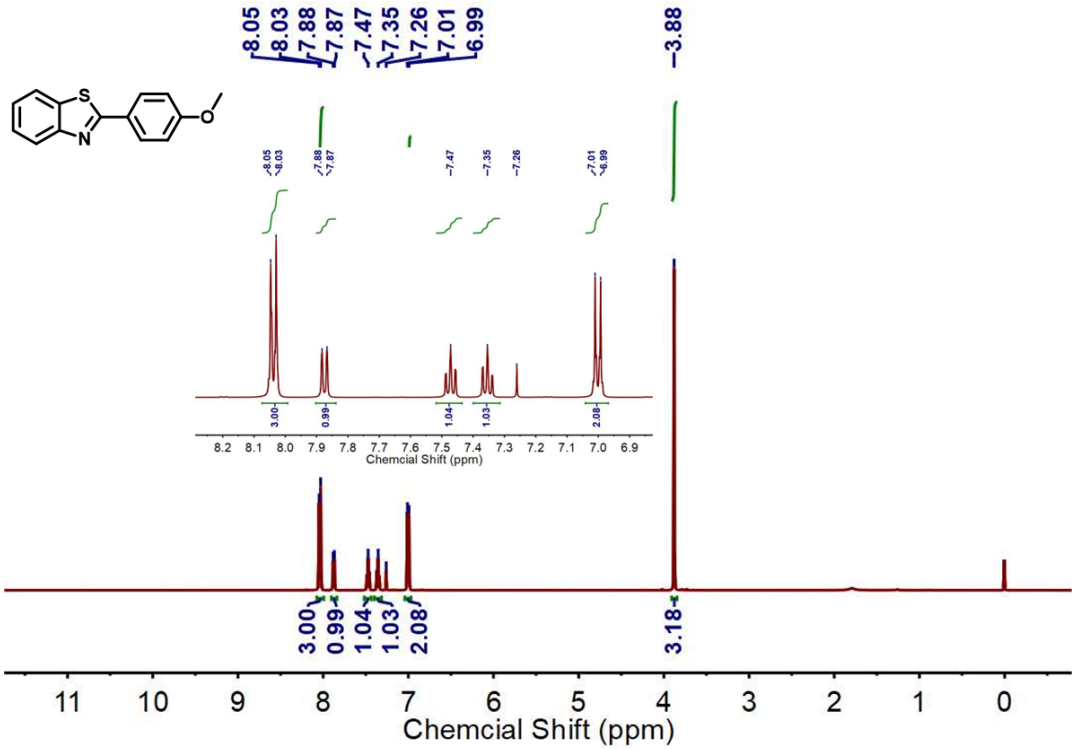

Figure S23. ^{1}H NMR spectrum of 2-(4-methoxyphenyl) benzo[*d*]thiazole (3c).

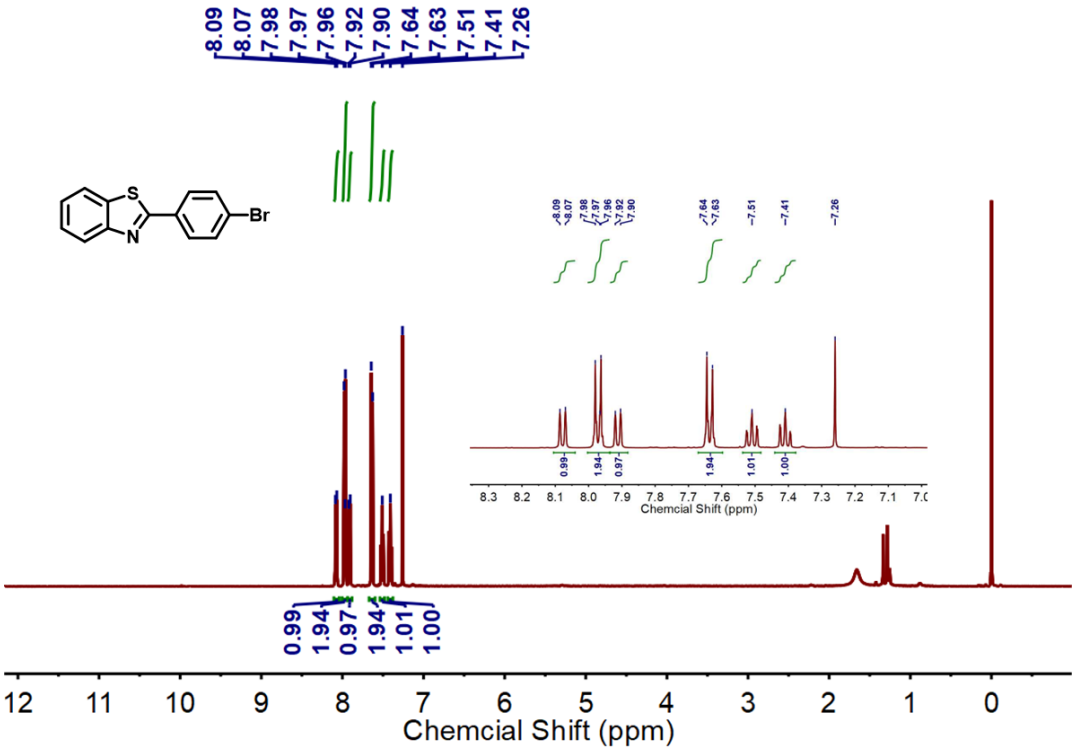

Figure S24. ^{1}H NMR spectrum of 2-(4-bromophenyl)benzo[*d*]thiazole (3d).

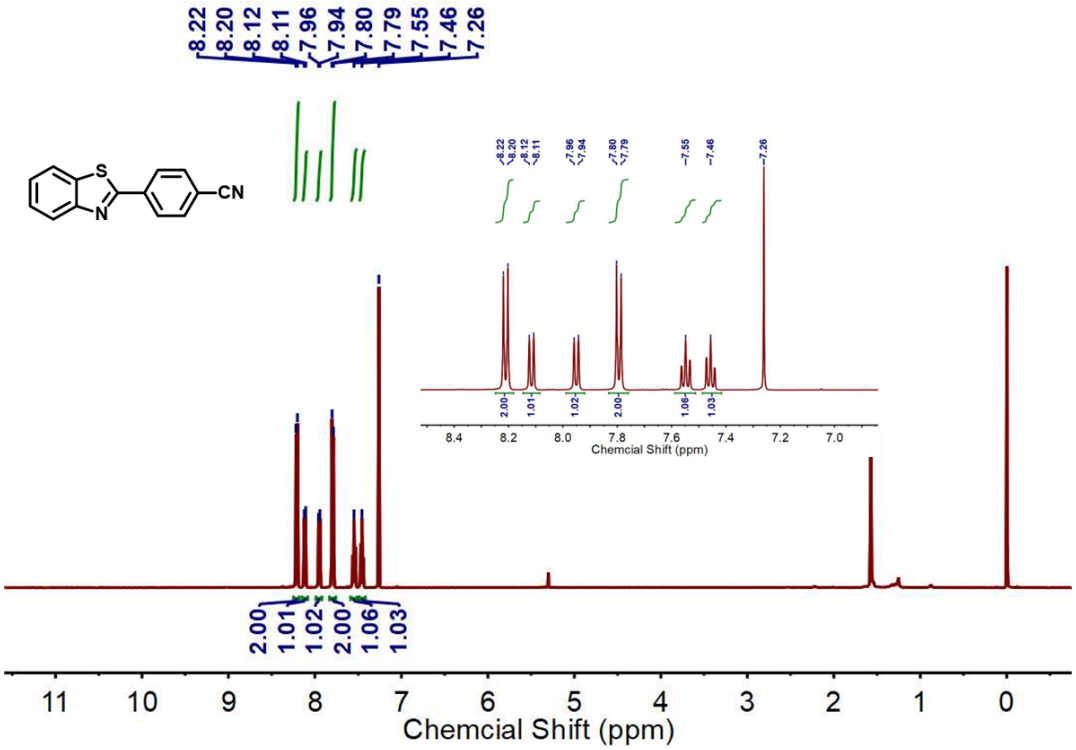

Figure S25. ^{1}H NMR spectrum of 4-(benzo[*d*]thiazol-2-yl)benzonitrile (3e).

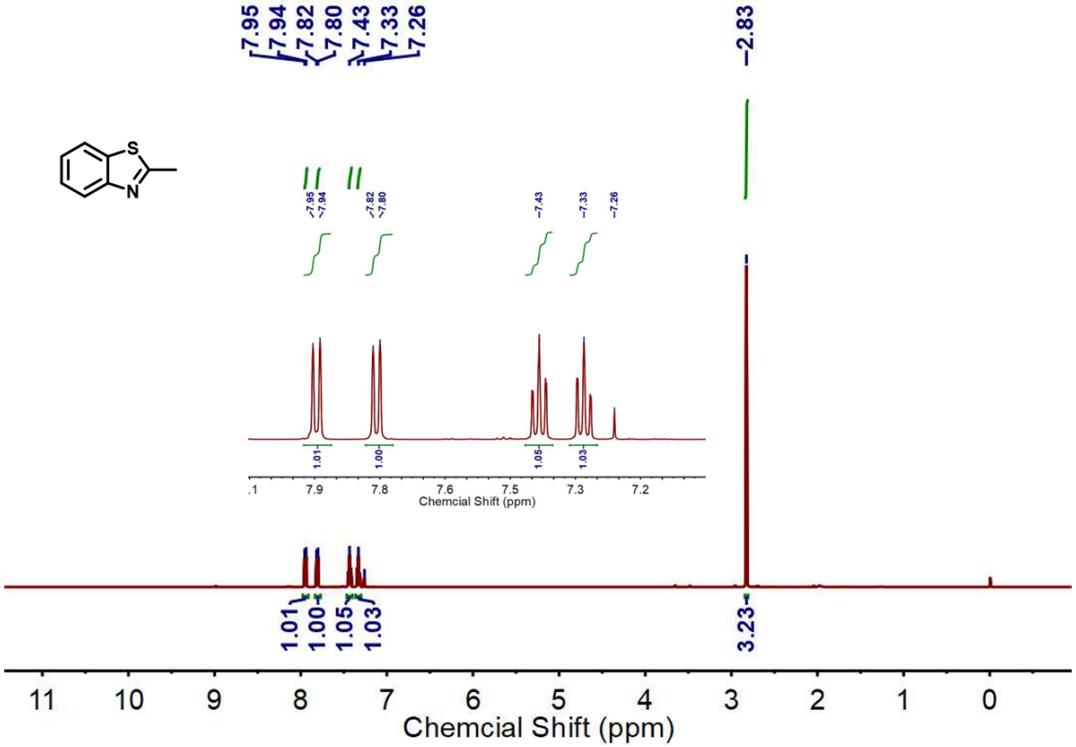

Figure S26. ^{1}H NMR spectrum of 2-methylbenzo[*d*]thiazole (f).

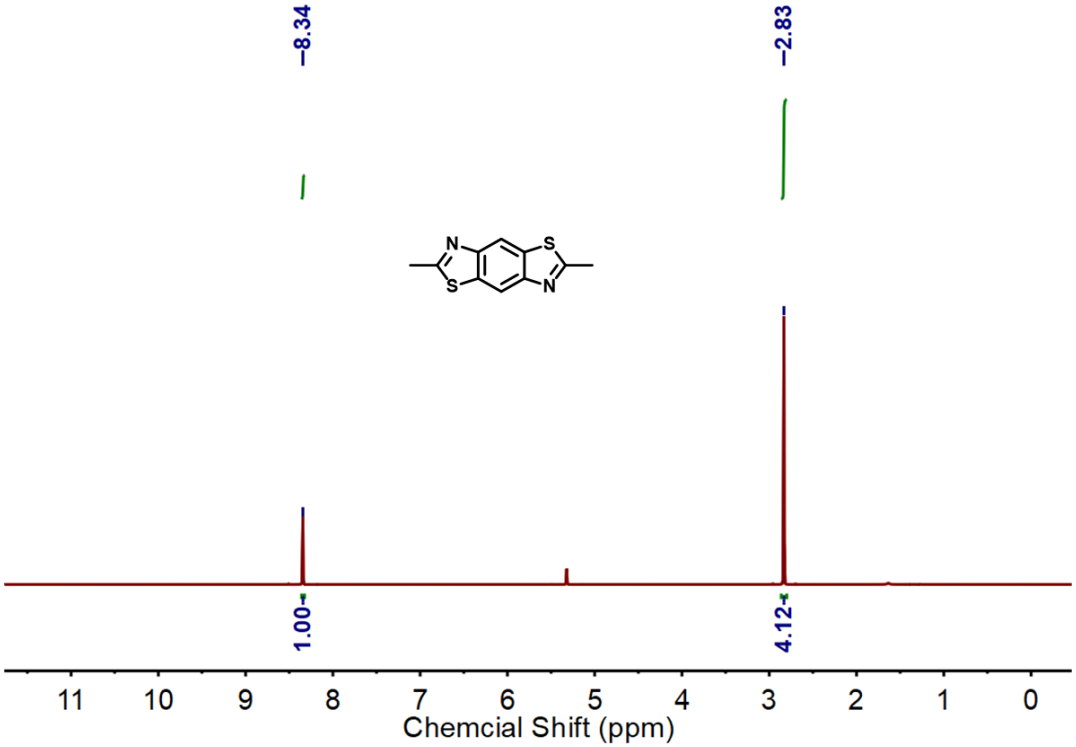

Figure S27. ^{1}H NMR spectrum of 2,6-dimethylbenzo[1,2-*d*:4,5-*d*']bis(thiazole) (3i).

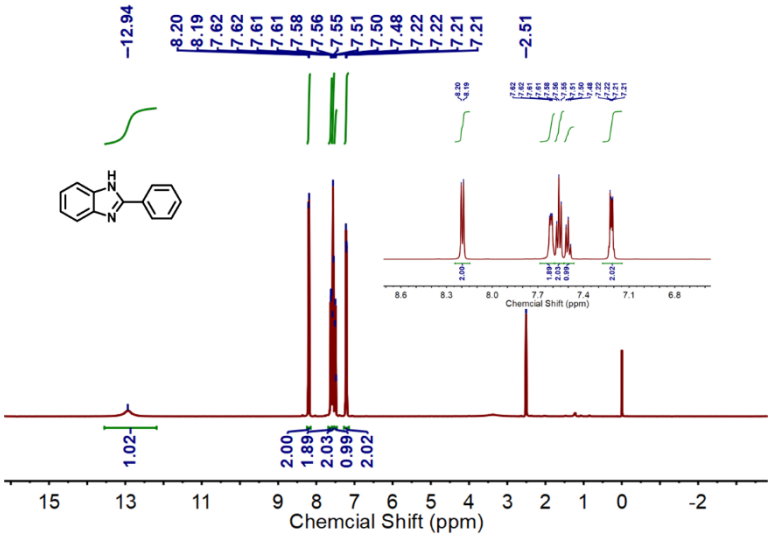

Figure S28. ^{1}H NMR spectrum of 2-phenyl-1H-benzo[d]imidazole (3n).

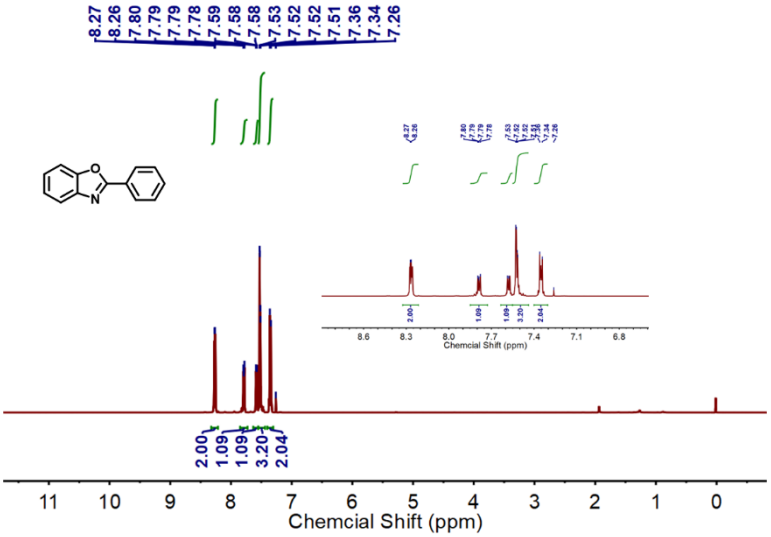

Figure S29. ^{1}H NMR spectrum of 2-phenylbenzo[d]oxazole (3o).

Reference

[1] Zhi, Q.; Liu, W.; Jiang, R.; Zhan, X.; Jin, Y.; Chen, X.; Yang, X.; Wang, K.; Cao, W.; Qi, D.; and Jiang, J. Piperazine-Linked Metalphthalocyanine Frameworks for Highly Efficient Visible-Light-Driven H_2O_2 Photosynthesis *J. Am. Chem. Soc.* **2022**, *144*, 46, 21328-21336.

[2] Wang, H.; Yang, C.; Chen, F.; Zheng, G.; and Han, Q. A Crystalline Partially Fluorinated Triazine Covalent Organic Framework for Efficient Photosynthesis of Hydrogen Peroxide. *Angew. Chem. Int. Ed.* **2022**, *61*, e202202328.

[3] Kou, M.; Wang, Y.; Xu, Y.; Ye, L.; Huang, Y.; Jia, B.; Li, H.; Ren, J.; Deng, Y.; Chen, J.; Zhou, Y.; Lei, K.; Wang, L.; Liu, W.; Huang, H.; and Ma, T. Molecularly Engineered Covalent Organic Frameworks for Hydrogen Peroxide Photosynthesis. *Angew. Chem. Int. Ed.* **2022**, e202200413.

[4] Krishnaraj, C.; Jena, H. S.; Bourda, L.; Laemont, A.; Pachfule, P.; Roeser, J.; Chandran, C. V.; Borgmans, S.; Rogge, S. M. J.; Leus, K.; Stevens, C. V.; Martens, J. A.; Speybroeck, V. V.; Breynaert, E.; Thomas, A.; and Voort, P. V. D. Strongly Reducing (Diarylamino)benzene-Based Covalent Organic Framework for Metal-Free Visible Light Photocatalytic H_2O_2 Generation *J. Am. Chem. Soc.* **2020**, *142*, 20107-20116.

[5] Chai, S.; Chen, X.; Zhang, X.; Fang, Y.; Sprick, R. S.; and Chen, X. Rational design of covalent organic frameworks for efficient photocatalytic hydrogen peroxide production. *Environ. Sci.: Nano,* **2022**, *9*, 2464-2469.

[6] Zhai, L.; Xie, Z.; Cui, C.; Yang, X.; Xu, Q.; Ke, X.; Liu, M.; Qu, L.-B.; Chen, X.; and Mi, L. Constructing Synergistic Triazine and Acetylene Cores in Fully Conjugated Covalent Organic Frameworks for Cascade Photocatalytic H_2O_2 Production. *Chem. Mater.* **2022**, *34*, 5232-5240.

[7] Wu, M.; Shan, Z.; Wang, J.; Liu, T.; Zhang, G. Three-dimensional covalent organic framework with *tty* topology for enhanced photocatalytic hydrogen peroxide production. *Chem. Eng. J.* **2023**, *454*, 140121.